Organic &
Biomolecular
Chemistry

Cite this: *Org. Biomol. Chem.*, 2011, **9**, 198

www.rsc.org/obc

PAPER

Guanidiniocarbonyl-pyrrole-aryl conjugates as nucleic acid sensors: switch of binding mode and spectroscopic responses by introducing additional binding sites into the linker†

Kathrin Gröger,[a] Domagoj Baretić,[b] Ivo Piantanida,*[b] Marko Marjanović,[c] Marijeta Kralj,[c] Marina Grabar,[d] Sanja Tomić[d] and Carsten Schmuck*[a]

Received 10th May 2010, Accepted 1st October 2010
DOI: 10.1039/c0ob00103a

Two novel guanidiniocarbonyl pyrrole–pyrene conjugates **3** and **4** as spectroscopic probes for ds-polynucleotides were synthesized and their interaction with different ds-DNAs/RNAs studied. Compared to a previously reported first set of conjugates (**1** and **2**) the significant extension and increased rigidity of the central part of the structure resulted in a switch of DNA binding mode from intercalative (previously studied derivatives **1** and **2** with a nonbinding and flexible linker) to minor groove binding of the two novel guanidiniocarbonyl-pyrrole–pyrene conjugates **3** and **4**. These two compounds interact strongly with ds-DNAs, but only weakly with ds-RNA. The newly incorporated heterocyclic moieties within the central part of the structure of **3** and **4** were able to control by steric and hydrogen-bonding effects the alignment of the molecules within various, structurally different forms of DNA minor grooves, whereby even small differences in the position of the attached pyrene within the groove were reflected in different fluorimetric responses. In addition, **3** and **4** revealed intriguing *in vitro* selectivity among various human tumour cell lines.

Introduction

Small molecules targeting DNA/RNA have attracted significant scientific interest due to the medicinal, biochemical and biological implications of such molecular recognition events.[1] Most often these small molecules rely on one dominant non-covalent binding mode for their interaction with double stranded (ds) DNA/RNA (*e.g.* intercalation, minor or major groove binding, external electrostatic binding).[2] However, the combination of different binding modes within one molecule as well as additional steric and structural features controlling three-dimensional recognition drew some attention over the last few years with the aim of developing new more selective drugs or biochemical markers as well as research tools on a molecular level. For instance, methods for sequence-specific detection of ds-DNA and ds-RNA are becoming increasingly useful and important as diagnostic and imaging tools, among which fluorescent techniques are representing about 60% of the detection enabling technologies used in molecular biology and medicine.[3] However, the design and synthesis of novel small molecules with multiple DNA/RNA-binding features within a structurally well defined architecture is still highly demanding. Within the last two years we have in this context developed guanidiniocarbonyl-pyrrole-aryl hybrid compounds in which a guanidiniocarbonyl pyrrole cation was connected *via* a flexible linker to an aromatic moiety.[4,5] Systematic studies of a series of such compounds were undertaken with the intention to a) determine the minimal size of the aryl-moiety necessary for efficient "anchoring" of the small molecule within ds-DNA/RNA by intercalation; b) to define structural properties (length, flexibility) of the linker between the guanidiniocarbonyl-pyrrole cation and the aryl group, which allows efficient binding of the cation to DNA/RNA after intercalation of the aromatic unit and c) to find an appropriate fluorescence probe to report the binding event in a selective manner. Up till now, we determined that for our compounds the minimal aryl-moiety required for efficient intercalation was acridine and a butyl linker provided sufficient length and flexibility to allow simultaneous intercalation of the aryl unit and groove binding of the cation.

Even more efficient for intercalation was a pyrene, and thus the two hybrid compounds **1** and **2** revealed selective and even sequence specific fluorescence responses to several different DNA or RNA sequences.[5] While the aliphatic, flexible linker in **1** was inert with respect to DNA/RNA interactions, the positive charge

[a]*Institute for Organic Chemistry, University of Duisburg-Essen, Universitässtrasse 7, 45141, Essen, Germany. E-mail: carsten.schmuck@uni-due.de; Fax: (+) 201 183 4259*
[b]*Division of Organic Chemistry and Biochemistry, "Ruđer Bošković" Institute, P. O. Box 180, HR-10002, Zagreb, Croatia. E-mail: Ivo.Piantanida@irb.hr*
[c]*Division of Molecular Medicine, "Ruđer Bošković" Institute, Zagreb, Croatia*
[d]*Laboratory for Chemical and Biological Crystallography, "Ruđer Bošković" Institute, P. O. Box 180, HR-10002, Zagreb, Croatia*
† Electronic supplementary information (ESI) available: CD titrations of ct-DNA with **3** and **4**. See DOI: 10.1039/c0ob00103a

This journal is © The Royal Society of Chemistry 2011

of the lysine side chain in the linker of a second generation compound **2** contributed significantly to DNA/RNA binding.[4,5] This was attributed to additional charge interactions with the nucleic acid backbone. This binding mode was also supported by preliminary molecular modelling studies of a **2**/poly dAdT-poly dAdT complex which hinted to the importance of anchoring the pyrene by intercalation into DNA in order to allow the accommodation of the guanidiniocarbonyl pyrrole moiety within the DNA minor groove. However, inspired by the previously noted RNA-specific fluorescence change of **1**, which was caused by pyrene-excimer formation within the RNA groove,[4] we have now designed and prepared two novel pyrenyl-guanidiniocarbonyl pyrrole hybrid compounds **3** and **4** (Scheme 1). In these compounds the linker between pyrene and the guanidinio-pyrrole moiety was significantly modified by introducing additional aromatic moieties next to the pyrene (a methyl imidazole in **3** or a pyrrole-methyl imidazole unit in **4**). These heterocycles themselves are able to interact with DNA/RNA as shown by Dervan and coworkers.[6] However, these building blocks also significantly rigidified the linker. Most likely a simultaneous intercalation of the pyrene into DNA/RNA and interactions of the linker within DNA/RNA grooves will not be possible. It was therefore expected that a competition between those two binding modes would occur and perhaps might be highly sensitive to the nucleic acid basepair composition and secondary structure.

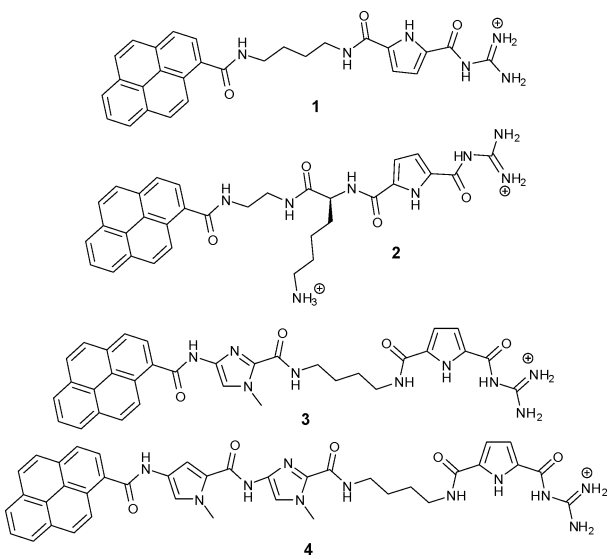

Scheme 1 Two previously studied (**1** and **2**) and two novel (**3** and **4**) guanidiniocarbonyl-pyrrole-aryl conjugates with different linkers.

Results and discussion

Synthesis

The syntheses of the novel hybrid compounds **3** and **4** were achieved by two analogous procedures as shown in Schemes 2 and 3. Compounds **6** and **14** which are necessary for both syntheses were prepared analogous to the method of Dervan *et al.*[7] and compound **12** was available according to a procedure reported earlier by us.[8]

The synthesis of compound **3** (Scheme 2) started with a standard coupling reaction between pyrene carboxylic acid **5** and the imidazole salt **6** by PyBOP activation. After the removal of the ethyl ester in **7** by basic hydrolysis the free acid **8** was activated with PyBOP and then reacted with *N*-Boc-protected 1,4-diaminobutane **9** to the protected compound **10**. Subsequently the Boc protecting group was removed from **10** by the use of trifluoroacetic acid (TFA) yielding the ammonium salt **11**, which was afterwards linked to the carboxylate **12** in a PyBOP activated coupling reaction. The desired end product **3** could then be obtained after a final deprotection using TFA. The preparation of compound **4** is shown in Scheme 3. The starting materials were an imidazole-pyrrole salt **14** and again pyrene carboxylic acid **5** which were coupled with the aid of PyBOP to obtain compound **15**. After a basic hydrolysis of the ethyl ester in **15** the PyBOP activated free acid **16** was treated with **9** to yield protected compound **17**. Boc-removal under acidic conditions (TFA) and a subsequent PyBOP mediated coupling reaction between compound **18** and ammonium salt **12** led to protected compound **19**. Finally TFA was used to remove the protecting group and the end product **4** could be isolated.

Physico-chemical and spectroscopic properties of aqueous solutions of 3 and 4

Compounds **3** and **4** were well soluble in water within a 10^{-4} mol dm^{-3} range and the absorbencies were found to be proportional to the concentration up to $c = 5 \times 10^{-5}$ mol dm^{-3} indicating that there is no significant intermolecular stacking which should give rise to hypochromicity effects. Absorption maxima and corresponding molar extinction coefficients (ε) are given in Table 1. In buffer at pH 7 and pH 5 UV/Vis spectra were identical to pure water. Heating of the aqueous solutions of either compound up to 90 °C did not yield any significant changes in the UV/Vis spectra proving the chemical stability of the compounds under these conditions.

According to the comparison of the absorption maxima (Table 1) with the previously prepared compounds **1** and **2**,[4,5] the maximum at λ = 295 nm could be attributed to the

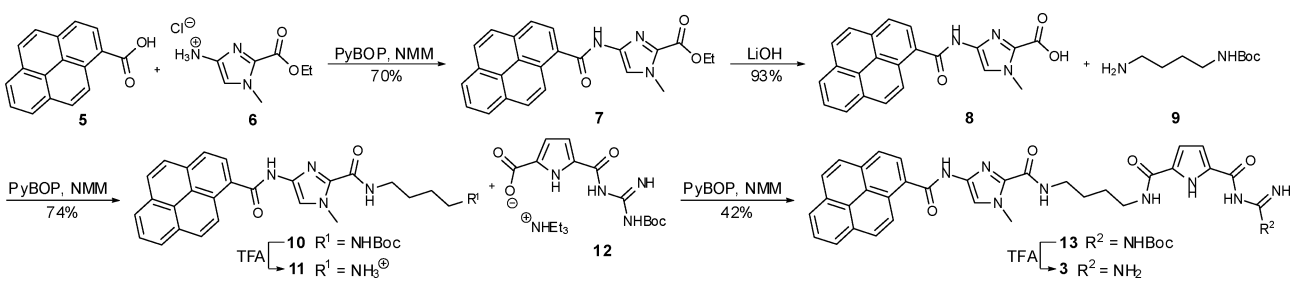

Scheme 2 Synthesis of compound **3**.

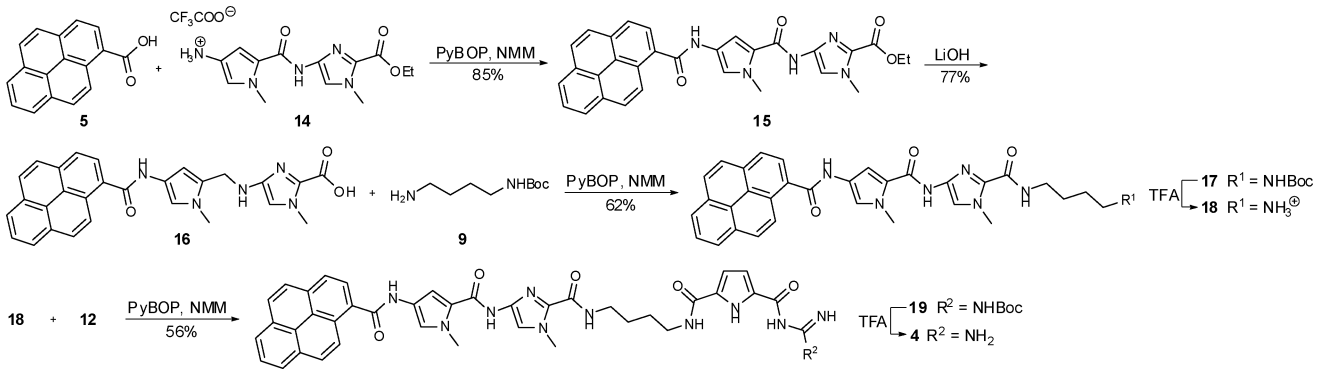

Scheme 3 Synthesis of compound **4**.

Table 1 Electronic absorption maxima and corresponding molar extinction coefficients of studied compounds in aqueous medium

	λ_{max}/nm ($\varepsilon \times 10^3$/dm^3 mol^{-1} cm^{-1})
1[a]	242 (24.2); 276 (38.1); 303 (28.1); 342 (20.4)
2[a]	231 (58.17); 242 (48.2); 276 (33.7); 307 (28.6); 344 (18.2); 377 (1.8)
3[b]	295 (29.9); 355 (22.5)
4[b]	295 (21); 355 (17.8)

[a] Previous results.[4,5] [b] Determined at pH 5 (sodium citrate buffer, $I = 0.03$ mol dm^{-3}) due to poor solubility at pH 7.

guanidiniocarbonyl pyrrole moiety, while the maximum at λ = 355 nm belongs to pyrene. A more detailed comparison of the data presented in Table 1 indicates more simplified UV/Vis spectra for **3** and **4** compared to **1** and **2**, most likely due to the overlapping of absorption bands of the guanidiniocarbonyl pyrrole cation with the absorption bands of the pyrrole and imidazole units incorporated into the linker.

Both **3** and **4** showed fluorescence emission, linearly dependent on the concentration of the compound in water up to $c = 5.0 \times 10^{-6}$ mol dm^{-3} (Fig. 1). At higher concentrations increase of fluorescence emission became non-proportional due to the inner filter effects. The fluorescence of **3** or **4** was weakly dependent on pH in the range pH = 3–8, most likely due to the reversible

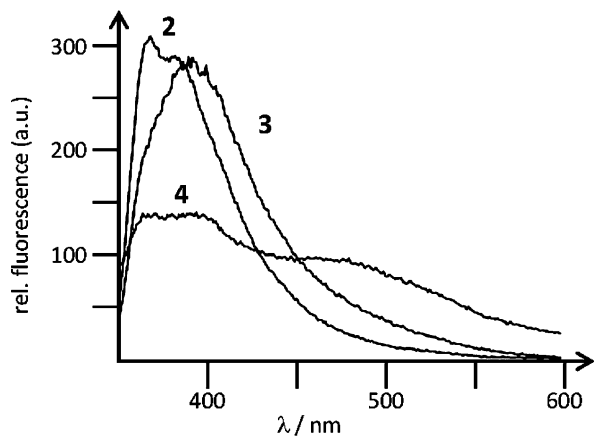

Fig. 1 Fluorescence emission spectra of **2** (λ_{exc} = 344 nm, $c = 1.0 \times 10^{-6}$ mol dm^{-3}), **3** (λ_{exc} = 355 nm, $c = 5.0 \times 10^{-7}$ mol dm^{-3}), **4** (λ_{exc} = 355 nm, $c = 2.0 \times 10^{-6}$ mol dm^{-3}), collected under the same instrument setup, at pH 5 (sodium citrate buffer, $I = 0.03$ mol dm^{-3}).

protonation and deprotonation of the guanidiniocarbonyl pyrrole moiety. This pH-dependent spectral change allowed us to estimate a p$K_a \approx 5.5$, indicating that at pH 7, **3** and **4** are less protonated than at pH 5.

Interactions with polynucleotides in water

Both **3** and **4** precipitated at pH 7 upon addition of any DNA and RNA studied at higher concentrations, which was not the case at pH 5 due to the better solubility of **3** and **4** caused by protonation of the guanidiniocarbonyl pyrrole moiety. Therefore all further experiments were done at pH 5.

Thermal denaturation experiments. At pH 5 compounds **3** and **4** stabilized ds-DNA somewhat weaker than previously studied compounds **1** or **2** (Table 2). Similar to their previously studied analogues, **3** and **4** did not stabilize ds-RNA. A more detailed analysis of stabilization effects revealed a strongly non-linear relationship between ΔT_m values and ratio r = [compound]/[ds-DNA], pointing toward saturation of the binding sites at about r = 0.2–0.3. Moreover, **4** stabilized both DNAs (ct-DNA and poly dA-poly dT) significantly stronger than **3**, most likely due to the additional interactions of the imidazole moiety present only in **4**. Comparable stabilization effects obtained for A-T polynucleotide and ct-DNA (42% G-C basepairs) by both **3** and **4** indicated that stabilization is not significantly dependent on the basepair composition of the polynucleotide.

Fluorimetric titrations of 3 and 4 with double stranded (ds-)polynucleotides. Although all compounds studied possess UV/vis bands at $\lambda > 300$ nm, UV/vis titrations were not applicable

Table 2 Thermal denaturation values (ΔT_m/°C)[a] of ds-polynucleotides upon addition of compounds **1–4** at ratio [b] r = 0.3, pH = 5.0 (sodium citrate buffer, $I = 0.03$ mol dm^{-3})

	1[e]	**2**[e]	**3**	**4**
ct-DNA	+7.2	+9.7	+4.0	+7.0
poly dA - poly dT	d	+11.7	+4.2	+7.3
poly rA - poly rU[c]	−1.5/0	0	0	0

[a] Error in ΔT_m: ±0.5 °C. [b] r = [compound]/[polynucleotide]. [c] Biphasic transitions: the first transition at T_m = 30.3 °C is attributed to denaturation of poly rA-poly rU and the second transition at T_m = 85.8 °C is attributed to denaturation of poly rAH$^+$-poly rAH$^+$ since poly rA at pH = 5 is mostly protonated and forms ds-polynucleotide.[9,10] [d] Not determined. [e] Previous results.[4,5]

 This journal is © The Royal Society of Chemistry 2011

for the study of their interactions with ds-polynucleotides since addition of ct-DNA yielded only minor changes in their UV/Vis spectra. Moreover, addition of some DNAs resulted in precipitation. However, fluorescence allowed titrations at significantly lower concentrations, at which no precipitation was observed. The changes of fluorescence emission of **3** and **4** were remarkably dependent on the type (*e.g.* DNA *vs.* RNA) and secondary structure of the polynucleotide added (Fig. 2, Table 3). Namely, emission of **3** was quenched by most ds-DNAs, with the exception of poly dA-poly dT, addition of which did not yield a measurable fluorescence change. In contrast to **3**, the fluorescence of **4** was increased by ct-DNA and poly dA-poly dT, while no significant emission changes were observed upon addition of alternating DNAs with dAdT and dGdC basepairs. The observed differences in the fluorimetric response could be related to both different secondary structures of the various polynucleotides and/or structural differences of the linker in **3** and **4**. Namely, shorter compound **3**, which

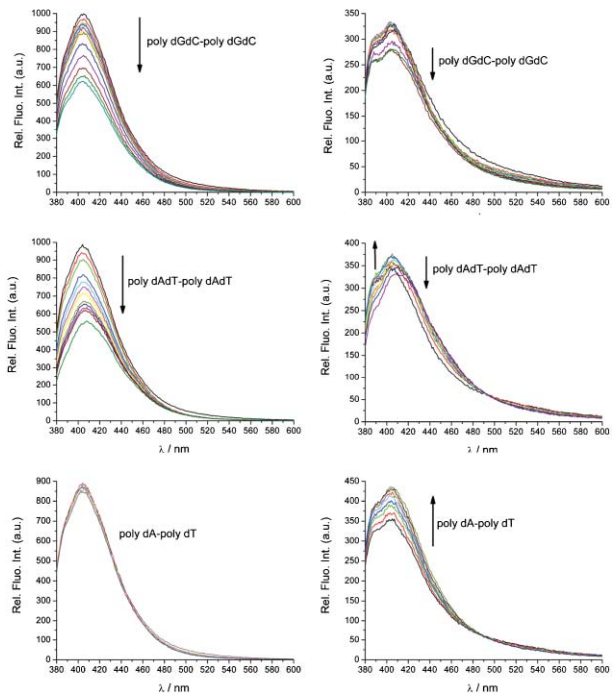

Fig. 2 Fluorimetric titrations of **3** (left column) and **4** (right column) (c(**3**, **4**) = 5.0×10^{-7} mol dm^{-3}, λ_{exc} = 355 nm) with various ds-polynucleotides at ratio r[compound]/[polynucleotide] = 0–0.01. Done at pH 5 (sodium citrate buffer, I = 0.03 M).

Table 3 The spectroscopic properties[a] of complexes of studied compounds with ds-polynucleotides observed in fluorimetric titrations at pH = 5 (sodium citrate buffer, I = 0.03 mol dm^{-3})

	poly dAdT - poly dAdT	poly dGdC - poly dGdC	poly dA - poly dT	poly rA - poly rU
3	[b]0.5	[b]0.7	1	1
4	1	[c]0.9	[b]1.3	[c]1.1

[a] Emission change; $I = I$(complex)/I(compd). [b] I(complex) obtained from Scatchard analysis of titration data. [c] I(complex) estimated from titration data since Scatchard analysis was not possible due to small changes, changes in opposite directions or linear change abruptly ending at well-defined intensity.

Table 4 Binding constants (logK_s), ratios n = [bound compound]/[polynucleotide] of studied compounds with ds-polynucleotides calculated from fluorimetric titrations at pH = 5 (sodium citrate buffer, I = 0.03 mol dm^{-3})[a]

	dAdT-dAdT logKs (n)	dGdC-dGdC logKs (n)	dAdT logKs (n)	rA-rU logKs (n)
2	6.5 (0.3)	6.3 (0.2)	[b]	5.4 (0.2)
3	6.0 (0.2)	5.5 (0.2)	[b]	[b]
4	[b]	[b]	6.9 (0.1)	[b]

[a] Titration data were processed using the Scatchard equation, accuracy of obtained $n \pm 10$–30%, consequently log K_s values vary in the same order of magnitude. [b] Too small changes or accurate calculation.

is characterized by a less rigid linker equipped with only one DNA-interacting moiety (methylimidazole) seems to fit better into the minor groove of classical β-helix DNA (here presented by alternating polynucleotides), whereby the fluorescence of pyrene is quenched. However, **4** due to its more rigid structure and the additional DNA-binding pyrrole moiety in the linker, binds better into the very narrow and deep minor groove of poly dA-poly dT, yielding an increase of pyrene fluorescence, while binding of **4** to alternating polynucleotides does not change the fluorescence of the pyrene moiety significantly.

The titration data with measurable fluorescence changes were processed by means of the Scatchard equation[11] using non-linear curve fitting procedures to obtain the binding constants and ratio $n_{[\text{bound compound}]/[\text{polynucleotide}]}$ (Table 4). Similar binding constants (logK_s = 5–6) suggest roughly comparative affinity of **3** and **4** toward most ds-DNAs, which also agrees well with the previously determined affinities of their close analogues **1** and **2**.[4,5]

CD spectroscopy. So far, non-covalent interactions at 25 °C were studied by monitoring the spectroscopic properties of **3** and **4** upon addition of the polynucleotides. In order to get more insight into the changes of polynucleotide properties induced by small molecule binding, we have chosen CD spectroscopy as a highly sensitive method toward conformational changes in the secondary structure of polynucleotides.[12] In addition, achiral small molecules can eventually acquire induced CD spectra (ICD) upon binding to polynucleotides, which could give useful information about their modes of interaction.[12,13] For example, the sign and magnitude of ICD bands can depend on the binding geometry: ligand–ligand stacking is expected to give strong bisignate exciton CD, minor groove binding to ds-DNA would orient the ligand approximately at 45° in respect to the chiral axis of DNA thus giving a strong positive ICD band, while intercalation should orient the aromatic moiety of the ligand co-planar with the basepairs giving rise to a weak ICD band (in most cases of a negative sign due to parallel orientation of the transition vector of the ligand and longer axis of surrounding basepairs).[14,15] Neither **3** nor **4** exhibit significant intrinsic CD spectra on their own at the experimental conditions used.

Interactions with ds-DNA. Addition of compounds **3** and **4** resulted in dramatic changes of the CD spectra of ds-DNAs, strongly dependent on the secondary structure of the DNA double helix (Fig. 3). Both **3** and **4** yielded strong positive ICD bands at λ = 300–310 nm and λ = 350–360 nm upon mixing with ct-DNA (not shown), poly dGdC-poly dGdC and poly dAdT-poly dAdT.

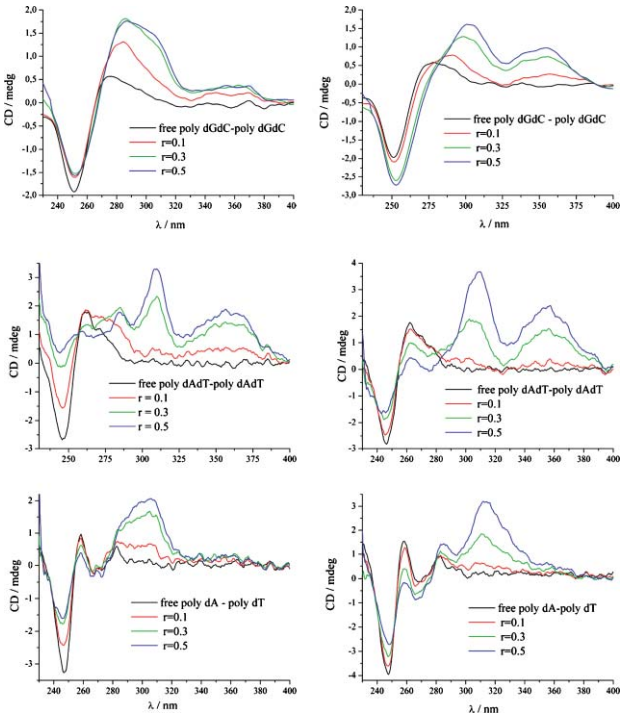

Fig. 3 Changes in the CD spectra of various polynucleotides ($c = 1.0 \times 10^{-5}$ mol dm^{-3}) upon addition of **3** (left column) or **4** (right column) at ratios r = [compound]/[polynucleotide] at pH 5.0 (sodium citrate buffer, $I = 0.03$ mol dm^{-3}).

In contrast to the aforementioned alternating ds-DNAs, mixing of **3** and **4** with poly dA-poly dT yielded only one strong positive ICD band at $\lambda = 300$–310 nm, while the other one (at $\lambda = 350$–360 nm) was not observed. Most likely the peculiar, twisted helix of poly dA-poly dT characterized by a much deeper and narrower minor groove in comparison with the classical β-helix of alternating ds-DNAs[10] hampered insertion of the large pyrene moiety, thus keeping it outside the chiral surroundings and suppressing the induction of a corresponding ICD band. Isoelliptic points in all titrations support formation of one dominant type of complex.

Opposite to ds-DNA, addition of any compound resulted in only minor changes in the positive bands of the ds-RNA polynucleotide (poly rA-poly rU, data not shown). The absence of any ICD band in all CD titrations with ds-RNA excludes a uniform orientation of **3** and **4** with respect to the chiral axis of ds-RNA.[12,14] The changes in the CD spectra were almost proportional to the ratio r, thus showing no saturation of binding sites even at an excess of compound over ds-RNA. These results suggest non-specific agglomeration of **3** and **4** along the ds-RNA helix caused by hydrophobic and electrostatic interactions.

Molecular modelling

The sensitivity of the fluorescence and ICD bands of **3** and **4** on various secondary structures of ds-DNA/RNA polynucleotides could be attributed to a fine interplay between rather rigid and structurally demanding compounds and differences in binding sites within the DNA/RNA studied. Since experimental results suggested that **3** and **4** bind within the DNA minor groove in contrast to the combined intercalative–minor groove binding of previously studied compound **2**, we performed molecular modelling studies of complexes of **2**, **3** and **4** bound to the well defined β-helical structure of poly dAdT-poly dAdT.

Results of molecular modelling for 2-polydAdT-polydAdT complex. The initial intercalative binding mode of **2** was not disrupted during the 12.5 ns of the MD simulations at room temperature. The analysis of the results of MD simulations showed that the pyrene moiety of **2** remained fully intercalated within ds-DNA, while the rest of the molecule formed several intermolecular hydrogen bonds with the DNA minor groove. In the final structure, after 12.5 ns of MD simulations, four such hydrogen bonds are present (Fig. 4). Two of them are formed between one terminal NH_2 group at the guanidiniocarbonyl pyrrole tail and the neighbouring nucleotide phosphate groups. The third hydrogen bond is observed between the aliphatic NH_3^+ functional group of **2** and the DNA phosphate group and the fourth hydrogen bond is formed between the amine group of the amide attached to the pyrene moiety of **2** and the deoxyribose from the neighbouring nucleobase. However, some other hydrogen bonds also appeared during MD simulations, and those present in the final structure appeared (randomly) at earlier stages of the simulation as well. For example, 500 ps after equilibration the intermolecular hydrogen bond between the terminal NH_2 group and neighbouring nucleobase was formed, and remained stable during the following 5 ns, followed by the formation of the hydrogen bond between the aliphatic NH_3^+ group of **2** and the neighbouring nucleotide phosphate group. The hydrogen bond between the second terminal NH_2 group of **2** and the neighbouring nucleotide phosphate group of ds-DNA was formed after 8 ns of MD simulation, and the intermolecular hydrogen bond between the amine group from the first amide bond from the pyrene moiety of **2** and the neighbouring nucleobase was formed at about 10 ns of MD simulation.

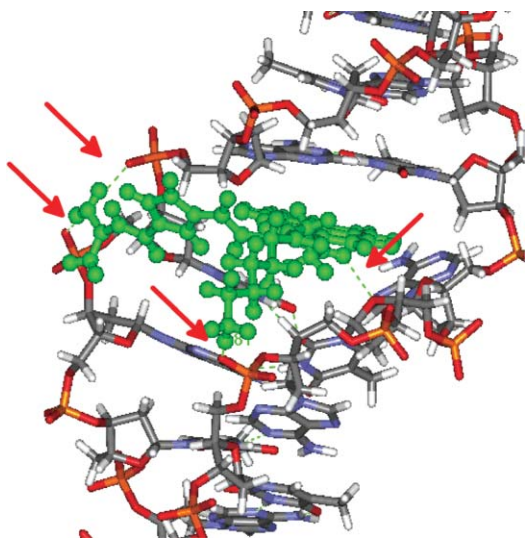

Fig. 4 The **2**/poly dAdT-poly dAdT complex obtained as a result of 12.5 ns of MD simulations. Red arrows indicate hydrogen bonds.

Apparently the intercalative binding of pyrene within ds-DNA was additionally stabilized by several hydrogen bonds within the DNA minor groove and to the phosphate backbone. The obtained structure of the **2**/poly dAdT-poly dAdT complex is in a good agreement with the previously published modelling studies of

 This journal is © The Royal Society of Chemistry 2011

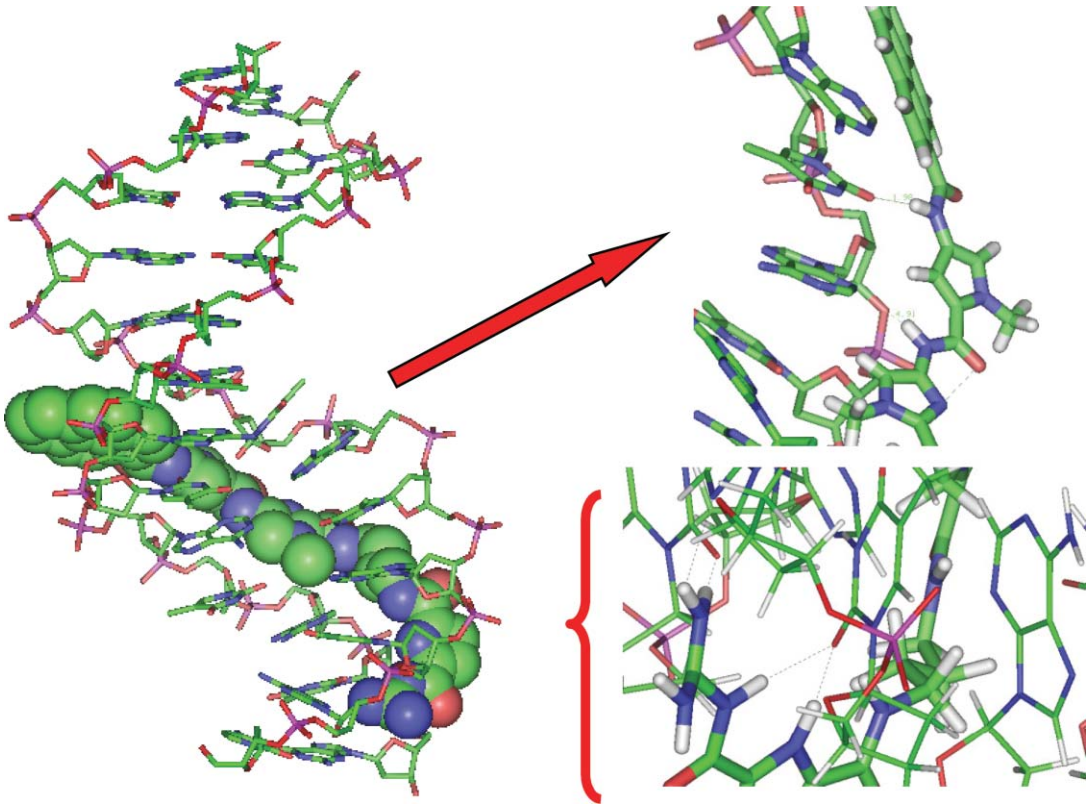

Fig. 5 Molecular modelling of **4**/poly dAdT-poly dAdT complex, left: complete structure, right: enlarged segments. Dotted grey lines indicate hydrogen bonds.

its close analogue **1** with DNA.[4,5] The additional electrostatic interaction of positively charged amine of **2** with the DNA correlates nicely to its stronger binding and thermal stabilization effect of **2** in comparison to **1**.[5]

Molecular modelling results for 3, 4-polydAdT-polydAdT complexes. Direct attachment of rigid imidazole (**3**) or pyrrole-imidazole (**4**) moiety to the pyrene dictated domination of one of two possible binding orientations: A) intercalation of the pyrene into DNA with no additional interactions of the linker and only limited interactions of the guanidiniocarbonyl-pyrrole cation with the nucleic acid or B) binding of the entire molecule into the DNA minor groove, whereby both the pyrrole or pyrrole-imidazole units in the linker as well as the guanidiniocarbonyl-pyrrole cation could form a number of binding interactions with the polynucleotide. Even the pyrene can form "edge-to-face" aromatic stacking interactions with the nucleobases in this binding mode. Molecular modelling results for **3** or **4**/poly dAdT-poly dAdT (Fig. 5) complexes yielded distinctively different results from those of the **2**/poly dAdT-poly dAdT complex, pointing toward more favourable interactions in the case of binding model B) in agreement with the above described spectroscopic result which also did not support an intercalation binding mode.

During 10.5 ns MD simulations, **3** and **4** remained stable in the poly dAdT-poly dAdT minor groove. In the final structure of the complexes, after 10.5 ns of MD simulations, there are several intermolecular hydrogen bonds: four in the **3**/poly dAdT-poly dAdT complex and five in the **4**/poly dAdT-poly dAdT complex. In the **3**/poly dAdT-poly dAdT complex the NH from the pyrrole ring of the guanidiniocarbonyl pyrrole tail forms hydrogen bonds with two neighbouring bases, namely with carbonyl oxygens of two thymine bases; the same oxygens are hydrogen bonded to the amine group from the amide bond between the pyrene moiety and the terminal guanidine. Besides, in the final structure the terminal NH_2 group of **3** has established NH-π interactions with the neighbouring base (guanine). The final **4**/poly dAdT-poly dAdT complex is stabilized by a hydrogen bond between the amide bond attached to the pyrene moiety of **4** and the neighbouring base (thymine carbonyl oxygen), by two hydrogen bonds between the terminal guanidine and the neighbouring DNA bases, adenine and thymine, combined with one additional hydrogen bond between NH from the terminal amide bond and the neighbouring base (thymine). In addition, pyrene forms twisted "edge-to-face" aromatic stacking interactions with the neighbouring adenine. In both complexes the carbonyl oxygen atoms of the linkers are pointing into the water. Apparently binding of **3** and **4** into the minor groove of poly dAdT-poly dAdT is additionally stabilized by the electrostatic interactions between phosphate groups of the polynucleotide and the positive side of the amide dipoles.

Biological activity

Compounds **3** and **4** were screened for their potential antiproliferative effects on a panel of 5 human cell lines, which were derived from different cancer types including HeLa (cervical carcinoma), MCF-7 (breast carcinoma), SW620 (colon carcinoma), MiaPaCa-2 (pancreatic carcinoma), and H460 (lung carcinoma) (Table 5).

Table 5 IC_{50} values (in μM)

	IC_{50}[a]				
	HeLa	MiaPaCa-2	SW 620	MCF-7	H 460
[b]**2**	15 ± 2	14 ± 0.02	92 ± 1	25 ± 1	52 ± 47
3	13 ± 2	14 ± 6	7 ± 2	77 ± 20	≥100
4	14 ± 1	18 ± 10	4 ± 1	14 ± 1	60 ± 39

[a] IC_{50}; the concentration that causes 50% growth inhibition. [b] Published results.[5]

Both **3** and **4** showed similar antiproliferative effects against the majority of cell lines similar to the previously studied **2**. A significant difference was observed on the SW 620 cell line, on which **3** and **4** revealed antiproliferative activity more than an order of magnitude higher compared to the effect of **2**. It is difficult to speculate about the mechanisms underlying this selectivity based just on the preliminary antiproliferative data presented here. However, a pronounced sensitivity of SW 620 cells is certainly an encouraging result for further more detailed biological studies, since this cell line represents a highly metastatic cell line, derived from a lymph node metastasis of a primary colon adenocarcinoma.

Conclusions

In this work the flexible and inert aliphatic linker of **2** was extended and rigidified by one (**3**) or two (**4**) heterocyclic moieties able to further interact with DNA and RNA by forming additional hydrogen bonds. Such an extension had profound impact on the DNA/RNA binding properties of the compounds. Both **3** and **4** interacted strongly with ds-DNAs, but only weakly with ds-RNA. Observed ICD bands at λ = 310 nm reveal that the guanidiniocarbonyl-pyrrole moiety of **3** and **4** is positioned within the minor groove of all ds-DNAs analogous to previously studied derivative **2**.[4] However, in contrast to the negative ICD bands at >330 nm attributed to intercalation of the pyrene of **2** into ds-DNA,[5] **3** and **4** with most ds-DNAs yielded positive ICD bands attributed to the pyrene moiety (λ = 330–350 nm), strongly indicating the positioning of pyrene within the minor groove of DNA double helix. Furthermore, positioning of **3** and **4** within the DNA minor groove was observed to be strongly dependent on the structural properties of the minor groove. This could explain the absence of any ICD band of the pyrene moiety of **3** and **4** for poly dA-poly dT, which is characterized by a peculiar, twisted helix and much narrower minor groove[16] in comparison to the more common β-helix of the other ds-DNAs.[10] Molecular modelling studies performed on poly dAdT-poly dAdT/**3** and **4** complexes revealed in more detail the nice structural fitting of complete molecules into the minor groove of the classical DNA β-helix, and in addition supported strong binding revealing the presence of at least 4–5 hydrogen bonds between **3** and **4** and DNA. Moreover, molecular modelling results revealed for both **3** and **4** possible "edge-to-face" aromatic interactions between pyrene and the DNA base pairs, which could be correlated to the different fluorimetric responses of **3** and **4** which depend on the structure of the DNA minor groove.

The most prominent consequence of the switch of the DNA binding mode from pyrene intercalation (previously studied compounds **1**, **2**) to pyrene minor groove binding (**3** and **4**), could be observed in the fluorimetric response. Namely, intercalating compounds either showed similar fluorimetric change for all ds-DNAs (**1**)[4] or fluorescence of **2** depended strongly on basepair composition due to different effects of aromatic stacking interactions between **2**-pyrene and A-T (fluorescence increase) *vs.* G-C basepairs (fluorescence quenching).[5] However, **3** and **4** reveal different fluorimetric response patterns in comparison to intercalative compounds, which is not sensitive to the DNA basepair composition but depends strongly on the structural features of the DNA minor groove. By ICD results, both **3** and **4** show similar patterns for all studied polynucleotides, however, ICD effects reflect only the binding position of parts of a molecule but do not describe in detail exact positioning as well as the surroundings of the bound molecule. However, fluorescence of pyrene is extremely polarity-sensitive and therefore it is extensively employed to characterize microheterogeneous systems. Consequently, small differences in the positioning of pyrene caused by structural differences in linker length and rigidity between **3** and **4** result in a fluorescence change of **3** only for the β-helical DNA minor groove but not for the peculiar deep and narrow minor groove of poly dA-poly dT,[16] while longer and more rigid molecule **4** reveals the opposite fluorescence response. Although the observed fluorimetric specificity is not accompanied by selective affinity, nevertheless it is to our knowledge unique fluorimetric sensing and therefore **3** and **4** could be considered as promising lead compounds for a further development of minor groove binders selective toward minor structural differences of various ds-DNA, especially those related to changes in A/T tracts.[17]

The antiproliferative effects of **3** and **4** are strongly dependent on the type of tumor cell line and span almost two orders of magnitude (from 2 μM–100 μM concentrations). Although observed activity cannot compete with the strongest drugs (active in nM range), nevertheless it points out that **3** and **4** efficiently cross the cell membrane and induce considerable biological effects. Thus, future modifications of the pyrene-guanidiniocarbonyl-pyrrole linkers of **3** and **4** by introduction of more groups, which could yield higher affinity, could result in more potent or selective compounds. Moreover, intriguing selectivity among different cell lines supports further detailed biological studies.

Experimental

Synthesis

General remarks. Solvents were dried and distilled under argon before use. The starting materials and reagents were used as obtained from *Aldrich*, *Fluka* or *Acros*. The NMR spectra were recorded at room temperature with a *Bruker* Avance 400 or a *Bruke*r DMX 600 NMR spectrometer. The chemical shifts are reported relative to the deuterated solvents. All IR spectra were measured as KBr pellets on a *Jasco* FT-IR 410 spectrophotometer. The ESI-HR-mass spectra were recorded on a *Bruker Daltonics* microTOF™ focus spectrometer and the EI-HR-mass on a *Finnigan* MAT 8200. Compounds **6** and **14** were prepared in analogy to the method of Dervan *et al.*[7] and compound **12** was available according to a procedure by Schmuck.[8]

 This journal is © The Royal Society of Chemistry 2011

Ethyl 1-methyl-4-(pyrene-1-carboxamido)-1*H*-imidazole-2-carboxylate (7). 1-Pyrenecarboxylic acid (**5**, 798 mg, 3.24 mmol), PyBOP (1.68 g, 3.24 mmol) and NMM (1.07 ml, 9.73 mmol) were dissolved in DMF (20 ml) and stirred for 30 min at room temperature to generate the active ester. After addition of the imidazole-salt (**6**, 1.00 g, 4.86 mmol) the reaction mixture was stirred for an additional 22 h at room temperature. Afterwards the solution was poured onto water (80 ml) and stirred for 2.5 h at 0 °C. The precipitated solid was filtered off and purified by flash chromatography (SiO_2, dichloromethane/ethyl acetate/hexane = 1/2/1). The desired product **7** (897 mg, 2.26 mmol, 70%) was obtained as a slightly yellow solid. Mp 211–214 °C; IR (KBr-pellet): ν_{max}/cm^{-1} = 2985 (w), 2954 (w), 2361 (s), 2339 (s), 1718 (m), 1655 (s), 1544 (s), 1374 (w), 1120 (s), 1073 (s), 462 (s); ^{1}H NMR (400 MHz, [D$_6$]DMSO, 25 °C): δ_H = 1.31 (t, 3H, J = 7.11 Hz, CH$_2$–C*H*$_3$), 4.03 (s, 3H, N–C*H*$_3$), 4.31 (q, 2H, J = 7.11 Hz, C*H*$_2$–CH$_3$), 7.92 (s, 1H, imidazole-C*H*), 8.14 (t, 1H, J = 7.64 Hz, pyrene-C*H*), 8.23–8.32 (m, 4H, pyrene-C*H*), 8.33–8.41 (m, 3H, pyrene-C*H*), 8.55 (d, 1H, J = 9.29 Hz, pyrene-C*H*), 11.44 (s, 1H, N*H*); ^{13}C NMR (150 MHz, [D$_6$]DMSO, 25 °C): δ_C = 14.1 (CH$_2$–*C*H$_3$), 35.6 (N–*C*H$_3$), 60.6 (*C*H$_2$–CH$_3$), 115.8 (imidazole-*C*H), 123.6, 123.8 (2 × pyrene-C_q), 124.4, 124.5, 125.8, 125.8, 126.0, 126.7, 127.2 (7 × pyrene-*C*H), 128.2 (pyrene-C_q), 128.3, 128.6 (2 × pyrene-*C*H), 130.1, 130.3, 130.7 (3 × pyrene-C_q), 131.2 (imidazole-C_q), 132.0 (pyrene-C_q), 137.7 (imidazole-C_q), 158.5, 166.4 (2 × *C*═O); HR-MS (EI) calcd. for $C_{24}H_{19}N_3O_3^{\bullet+}$ [M]$^{\bullet+}$: 397.14209, found: 397.14218.

1-Methyl-4-(pyrene-1-carboxamido)-1*H*-imidazole-2-carboxylic acid (8). The imidazole carboxylate (**7**, 841 mg, 2.12 mmol) and lithium hydroxide (267 mg, 6.36 mmol) were dissolved in THF/water (V_1:V_2 = 4 : 1, 25 ml) and stirred for 5.5 h at room temperature. Afterwards the solution was acidified with 5% hydrochloric acid to pH = 1 and immediately a solid precipitated. It was filtered off and lyophilised from water (15 ml) yielding **8** (728 mg, 1.97 mmol, 93%) as a slightly yellow solid. Mp > 230 °C; IR (KBr-pellet): ν_{max}/cm^{-1} = 2923 (w), 2361 (s), 2339 (s), 1657 (m), 1560 (s), 1544 (m), 1075 (m), 464 (s); ^{1}H NMR (400 MHz, [D$_6$]DMSO, 25 °C): δ_H = 4.02 (s, 3H, N–C*H*$_3$), 7.87 (s, 1H, imidazole-C*H*), 8.14 (t, 1H, J = 7.64 Hz, pyrene-C*H*), 8.23–8.32 (m, 4H, pyrene-C*H*), 8.33–8.41 (m, 3H, pyrene-C*H*), 8.54 (d, 1H, J = 9.29 Hz, pyrene-C*H*), 11.36 (s, 1H, N*H*); ^{13}C NMR (100 MHz, [D$_6$]DMSO, 25 °C): δ_C = 35.6 (N–*C*H$_3$), 115.5 (imidazole-*C*H), 123.6, 123.8 (2 × pyrene-C_q), 124.4, 124.5, 125.7, 125.9, 126.1, 126.6, 127.2 (7 × pyrene-*C*H), 128.1 (pyrene-C_q), 128.3, 128.5 (2 × pyrene-*C*H), 130.1, 130.5, 130.7, 131.9 (4 × pyrene-C_q), 132.1, 137.4 (2 × imidazole-C_q), 160.1, 166.4 (2 × *C*═O); HR-MS (pos. ESI) calcd. for $C_{21}H_{16}N_3O^+$ [M − CO$_2$ + H]$^+$: 326.12879, found: 326.12783.

***tert*-Butyl 4-(1-methyl-4-(pyrene-1-carboxamido)-1*H*-imidazole-2-carboxamido)-butylcarbamate (10).** The carboxylic acid (**8**; 745 mg, 2.02 mmol), PyBOP (1.05 g, 2.02 mmol) and NMM (0.67 ml, 6.09 mmol) were dissolved in DMF (12 ml) and stirred for 30 min at room temperature to generate the active ester. After addition of the amine (**9**, 761 mg, 4.04 mmol), the reaction mixture was stirred for an additional 20 h at room temperature. Afterwards the solution was poured onto water (40 ml) and stirred for 1.5 h at 0 °C. The precipitated solid was filtered off and purified by flash chromatography (SiO_2, ethyl acetate/hexane = 4/1). The desired product **10** (809 mg, 1.50 mmol, 74%) was obtained as a slightly yellow solid. Mp 106–107 °C; IR (KBr-pellet): ν_{max}/cm^{-1} = 3039 (w), 2935 (m), 2865 (w), 1685 (s), 1655 (s), 1528 (s), 1365 (m), 1168 (s), 849 (s), 470 (m); ^{1}H NMR (400 MHz, [D$_6$]DMSO, 25 °C): δ_H = 1.33–1.44 (m, 2H, imidazole-CO-NH-CH$_2$-C*H*$_2$-CH$_2$-CH$_2$), 1.36 (s, 9H, C*H*$_3$, ^{t}Bu), 1.44–1.54 (m, 2H, imidazole-CO-NH-CH$_2$-CH$_2$-C*H*$_2$-CH$_2$), 2.92 (q, 2H, J = 6.46 Hz, imidazole-CO-NH-C*H*$_2$-CH$_2$-CH$_2$-CH$_2$), 3.24 (q, 2H, J = 6.45 Hz, imidazole-CO-NH-CH$_2$-CH$_2$-CH$_2$-CH$_2$), 4.02 (s, 3H, N–C*H*$_3$), 6.79 (br. t, 1H, J = 5.19 Hz, N*H*), 7.76 (s, 1H, imidazole-C*H*), 7.98 (br. t, 1H, J = 6.04 Hz, N*H*), 8.14 (t, 1H, J = 7.65 Hz, pyrene-C*H*), 8.21–8.32 (m, 4H, pyrene-C*H*), 8.33–8.41 (m, 3H, pyrene-C*H*), 8.51 (d, 1H, J = 9.28 Hz, pyrene-C*H*), 11.09 (s, 1H, N*H*);^{13}C NMR (100 MHz, [D$_6$]DMSO, 25 °C): δ_C = 26.6 (imidazole-CO-NH-CH$_2$-CH$_2$-CH$_2$-CH$_2$), 27.0 (imidazole-CO-NH-CH$_2$-CH$_2$-CH$_2$-CH$_2$), 28.2 (3C, *C*H$_3$, ^{t}Bu), 35.0 (N–*C*H$_3$), 38.1 (imidazole-CO-NH-CH$_2$-CH$_2$-CH$_2$-CH$_2$), 39.6 (imidazole-CO-NH-CH$_2$-CH$_2$-CH$_2$-CH$_2$), 77.3 (C_q, ^{t}Bu), 114.6 (imidazole-*C*H), 123.6, 123.8 (2 × pyrene-C_q), 124.4, 124.4, 125.6, 125.7, 125.9, 126.6, 127.2 (7 × pyrene-*C*H), 128.1 (pyrene-C_q), 128.3, 128.5 (2 × pyrene-*C*H), 130.1, 130.7, 130.7, 131.9 (4 × pyrene-C_q), 134.4, 136.1 (2 × imidazole-C_q), 155.6, 158.6, 166.5 (3 × *C*═O); HR-MS (pos. ESI) calcd. for $C_{31}H_{34}N_5O_4^+$ [M + H]$^+$: 540.26053, found: 540.25907.

4-(1-Methyl-4-(pyrene-1-carboxamido)-1*H*-imidazole-2-carboxamido)butan-1-ammonium 2,2,2-trifluoroacetate (11). The protected precursor **10** (704 mg, 1.30 mmol) was dissolved in TFA (7 ml) and stirred at room temperature for 7 h. After removal of remaining TFA under reduced pressure, the residual oil was lyophilised from water (10 ml). The desired product **11** (719 mg, 1.30 mmol, quant.) was obtained as a slightly yellow solid. Mp 144 °C; IR (KBr-pellet): ν_{max}/cm^{-1} = 2361 (w), 2339 (w), 1677 (s), 1559 (s), 1370 (w), 1203 (s), 1137 (s), 720 (m), 454 (m); ^{1}H NMR (400 MHz, [D$_6$]DMSO, 25 °C): δ_H = 1.51–1.61 (m, 4H, imidazole-CO-NH-CH$_2$-CH$_2$-CH$_2$-CH$_2$), 2.76–2.88 (m, 2H, imidazole-CO-NH-CH$_2$-CH$_2$-CH$_2$-CH$_2$), 3.23–3.34 (m, 2H, imidazole-CO-NH-CH$_2$-CH$_2$-CH$_2$-CH$_2$), 4.03 (s, 3H, N–C*H*$_3$), 7.68 (br. s, 1H, N*H*$_2$), 7.77 (s, 1H, imidazole-C*H*), 8.01 (br. t, 1H, J = 6.15 Hz, N*H*), 8.14 (t, 1H, J = 7.15 Hz, pyrene-C*H*), 8.20–8.26 (m, 1H, pyrene-C*H*), 8.26–8.33 (m, 3H, pyrene-C*H*), 8.35–8.43 (m, 3H, pyrene-C*H*), 8.59 (d, 1H, J = 9.28 Hz, pyrene-C*H*), 11.04 (s, 1H, N*H*); ^{13}C NMR (100 MHz, [D$_6$]DMSO, 25 °C): δ_C = 24.5 (imidazole-CO-NH-CH$_2$-CH$_2$-CH$_2$-CH$_2$), 26.2 (imidazole-CO-NH-CH$_2$-CH$_2$-CH$_2$-CH$_2$), 35.0 (N–*C*H$_3$), 37.7 (imidazole-CO-NH-CH$_2$-CH$_2$-CH$_2$-CH$_2$), 38.6 (imidazole-CO-NH-CH$_2$-CH$_2$-CH$_2$-CH$_2$), 114.9 (imidazole-*C*H), 123.6, 123.8 (2 × pyrene-C_q), 124.4, 124.4, 125.6, 125.7, 126.0, 126.7, 127.2 (7 × pyrene-*C*H), 128.1 (pyrene-C_q), 128.3, 128.5 (2 × pyrene-*C*H), 130.1, 130.7, 130.8, 131.9 (4 × pyrene-C_q), 134.3, 136.0 (2 × imidazole-C_q), 158.0, 158.4 (2 × C_q, CF_3COO^-), 158.8, 166.6 (2 × *C*═O); HR-MS (pos. ESI) calcd. for $C_{26}H_{26}N_5O_2^+$ [M]$^+$: 440.20810, found: 440.20851.

***N*^{2}-(*N*-(*tert*-Butoxycarbonyl)carbamimidoyl)-*N*^{5}-(4-(1-methyl-4-(pyrene-1-carbox-amido)-1*H*-imidazole-2-carboxamido)butyl)-1*H*-pyrrole-2,5-dicarboxamide.** The salt **11** (103 mg, 0.19 mmol), the carboxylate (**12**; 74.0 mg, 0.19 mmol), PyBOP (98.8 mg, 0.19 mmol) and NMM (65 µl, 0.59 mmol) were dissolved in DMF (1.5 ml) and stirred for 72 h at room temperature. Afterwards the

solution was poured onto water (6 ml) and stirred 2 h at 0 °C. The precipitated solid was filtered off, lyophilised from water (5 ml) and purified by flash chromatography (SiO_2, ethyl acetate). The desired product **13** (99.1 mg, 0.14 mmol, 74%) was obtained as a yellow solid. Mp 204–205 °C (degradation); IR (KBr-pellet): ν_{max}/cm^{-1} = 2925 (m), 1728 (m), 1637 (s), 1532 (s), 1467 (s), 1369 (m), 1293 (s), 1237 (s), 1147 (s), 847 (m), 756 (m), 593 (w); ^{1}H NMR (400 MHz, [D$_6$]DMSO, 25 °C): δ_H = 1.44 (s, 9H, C*H*$_3$, ^{t}Bu), 1.50–1.60 (m, 4H, imidazole-CO-NH-CH$_2$-CH$_2$-CH$_2$-CH$_2$), 3.21–3.30 (m, 4H, imidazole-CO-NH-CH$_2$-CH$_2$-CH$_2$-CH$_2$), 4.02 (s, 3H, N–C*H*$_3$), 6.73–6.88 (m, 2H, pyrrole-C*H*), 7.76 (s, 1H, imidazole-C*H*), 8.01 (br. t, 1H, J = 6.04 Hz, N*H*), 8.14 (t, 1H, J = 7.65 Hz, pyrene-C*H*), 8.21–8.31 (m, 4H, pyrene-C*H*), 8.31–8.34 (m, 1H, N*H*), 8.34–8.40 (m, 3H, pyrene-C*H*), 8.52 (d, 1H, J = 9.29 Hz, pyrene-C*H*), 8.55 (br. s, 1H, N*H*), 9.30 (br. s, 1H, N*H*), 11.05 (br. s, 1H, N*H*), 11.08 (s, 1H, N*H*), 11.15 (br. s, 1H, N*H*); ^{13}C NMR (100 MHz, [D$_6$]DMSO, 25 °C): δ_C = 26.7 (imidazole-CO-NH-CH$_2$-CH$_2$-CH$_2$-CH$_2$), 26.8 (imidazole-CO-NH-CH$_2$-CH$_2$-CH$_2$-CH$_2$), 27.7 (3C, *C*H$_3$, ^{t}Bu), 35.0 (N–*C*H$_3$), 38.1 (imidazole-CO-NH-CH$_2$-CH$_2$-CH$_2$-CH$_2$), 38.4 (imidazole-CO-NH-CH$_2$-CH$_2$-CH$_2$-CH$_2$), 59.7 (C_q, ^{t}Bu), 111.6 (imidazole-*C*H), 114.6, 114.6 (2 × pyrrole-*C*H), 123.6, 123.8 (2 × pyrene-C_q), 124.4, 124.4, 125.6, 125.7, 125.9, 126.6, 127.2 (7 × pyrene-*C*H), 128.1 (pyrene-C_q), 128.3, 128.5 (2 × pyrene-*C*H), 130.1, 130.7, 130.7, 131.9 (4 × pyrene-C_q), 134.4, 136.1 (2 × imidazole-C_q), 158.4, 158.6, 159.5, 166.5 (4 × *C*═O); HR-MS (pos. ESI) calcd. for $C_{38}H_{40}N_9O_6^+$ [M + H]$^+$: 718.30961, found: 718.30996.

Amino(5-(4-(1-methyl-4-(pyrene-1-carboxamido)-1*H*-imidazole-2-carboxamido)-butylcarbamoyl)-1*H*-pyrrole-2-carboxamido)methaniminium 2,2,2-trifluoroacetate (3). The protected hybrid compound **13** (85.0 mg, 0.12 mmol) was dissolved in DCM/TFA (V_1:V_2 = 1 : 1, 3 ml) and stirred at room temperature for 5 h. After removal of DCM and remaining TFA under reduced pressure, the residual oil was lyophilised from water (3 ml) and purified by flash chromatography (MPLC, RP-18, methanol/water = 7/3, + 0.1% TFA) The desired product **3** (52.9 mg, 72.3 μmol, 60%) was obtained as a yellow solid. Mp 136–138 °C; IR (KBr-pellet): ν_{max}/cm^{-1} = 2950 (w), 2873 (w), 1702 (s), 1675 (s), 1542 (s), 1474 (m), 1365 (w), 1283 (s), 1200 (s), 1135 (m), 849 (m), 759 (m), 718 (m), 445 (m); ^{1}H NMR (400 MHz, [D$_6$]DMSO, 25 °C): δ_H = 1.50–1.60 (m, 4H, imidazole-CO-NH-CH$_2$-CH$_2$-CH$_2$-CH$_2$), 3.24–3.33 (m, 4H, imidazole-CO-NH-CH$_2$-CH$_2$-CH$_2$-CH$_2$), 4.02 (s, 3H, N–C*H*$_3$), 6.84–6.88 (m, 1H, pyrrole-C*H*), 7.02–7.06 (m, 1H, pyrrole-C*H*), 7.76 (s, 1H, imidazole-C*H*), 8.03 (br. t, 1H, J = 6.08 Hz, N*H*), 8.14 (t, 1H, J = 7.66 Hz, pyrene-C*H*), 8.17–8.32 (m, 8H, pyrene-C*H*, N*H*$_2$ and N*H*$_2^+$), 8.32–8.40 (m, 3H, pyrene-C*H*), 8.43 (br. t, 1H, J = 5.76 Hz, N*H*), 8.50 (d, 1H, J = 9.27 Hz, pyrene-C*H*), 11.02 (br. s, 1H, N*H*), 11.07 (s, 1H, N*H*), 12.34 (br. s, 1H, N*H*);^{13}C NMR (100 MHz, [D$_6$]DMSO, 25 °C): δ_C = 26.5 (imidazole-CO-NH-CH$_2$-CH$_2$-CH$_2$-CH$_2$), 26.8 (imidazole-CO-NH-CH$_2$-CH$_2$-CH$_2$-CH$_2$), 35.0 (N–*C*H$_3$), 38.0 (imidazole-CO-NH-CH$_2$-CH$_2$-CH$_2$-CH$_2$), 38.5 (imidazole-CO-NH-CH$_2$-CH$_2$-CH$_2$-CH$_2$), 112.2 (imidazole-*C*H), 114.7, 115.4 (2 × pyrrole-*C*H), 123.6, 123.8 (2 × pyrene-C_q), 124.4, 124.4 (2 × pyrene-*C*H), 125.3 (pyrrole-C_q), 125.6, 125.7, 126.0, 126.6, 127.2 (5 × pyrene-*C*H), 128.1 (pyrene-C_q), 128.3, 128.5 (2 × pyrene-*C*H), 130.1, 130.7, 130.7, 131.9 (4 × pyrene-C_q), 132.8 (pyrrole-C_q), 134.4, 136.1 (2 × imidazole-C_q), 155.0 (guanidine-C_q), 158.7, 159.0, 159.6, 166.5 (4 × *C*═O); HR-MS (pos. ESI) calcd. for $C_{33}H_{32}N_9O_4^+$ [M]$^+$: 618.25718, found: 618.25638; HPLC, LC-18 reversed phase, gradient: methanol/water = 7/3 → methanol/water = 10/0, + 0.1% TFA): 290 nm: retention time 11.40 min, relative area 98.03% → corrected yield: 51.9 mg, 70.9 μmol, 59%; 220 nm: retention time 11.39 min, relative area 87.61% → corrected yield: 46.3 mg, 63.3 μmol, 53%.

Ethyl 1-methyl-4-(1-methyl-4-(pyrene-1-carboxamido)-1*H*-pyrrole-2-carbox-amido)-1*H*-imidazole-2-carboxylate (15). 1-Pyrenecarboxylic acid (**5**; 273 mg, 1.11 mmol), the pyrrole salt (**14**; 450 mg, 1.11 mmol), PyBOP (578 mg, 1.11 mmol) and NMM (0.37 ml, 3.37 mmol) were dissolved in DMF (10 ml) and stirred for 23 h at room temperature. Afterwards the solution was poured onto water (40 ml) and stirred 4 h at 0 °C. The precipitated solid was filtered off, lyophilised from water (10 ml) and purified by flash chromatography (SiO_2, dichloromethane/ethyl acetate/hexane = 1/2/1). The desired product **15** (488 mg, 0.94 mmol, 85%) was obtained as a slightly yellow solid. Mp 156–157 °C; IR (KBr-pellet): ν_{max}/cm^{-1} = 3044 (w), 2954 (w), 2923 (w), 2855 (w), 2366 (w), 2339 (w) 1709 (s), 1655 (s), 1543 (s), 1428 (m), 1400 (m), 1369 (w), 1270 (m), 1125 (m), 849 (s), 484 (m); ^{1}H NMR (400 MHz, [D$_6$]DMSO, 25 °C): δ_H = 1.29 (t, 3H, J = 7.11 Hz, CH$_2$-C*H*$_3$), 3.95 (s, 6H, N–C*H*$_3$, imidazole and N–C*H*$_3$, pyrrole), 4.28 (q, 2H, J = 7.11 Hz, C*H*$_2$–CH$_3$), 7.21 (d, 1H, J = 1.86 Hz, pyrrole-C*H*), 7.60 (d, 1H, J = 1.76 Hz, pyrrole-C*H*), 7.70 (s, 1H, imidazole-C*H*), 8.14 (t, 1H, J = 7.65 Hz, pyrene-C*H*), 8.20–8.31 (m, 4H, pyrene-C*H*), 8.34–8.42 (m, 3H, pyrene-C*H*), 8.49 (d, 1H, J = 9.27 Hz, pyrene-*CH*), 10.73 (s, 1H, N*H*), 10.79 (s, 1H, N*H*).^{13}C NMR (100 MHz, [D$_6$]DMSO, 25 °C): δ_C = 14.1 (CH$_2$–*C*H$_3$), 35.4 (N–*C*H$_3$, imidazole), 36.4 (N–*C*H$_3$, pyrrole), 60.5 (CH$_2$–*C*H$_3$), 105.6 (pyrrole-*C*H), 115.5 (imidazole-*C*H), 119.8 (pyrrole-*C*H), 122.0, 122.4 (2 × pyrrole-C_q), 123.7, 123.8 (2 × pyrene-C_q), 124.4, 124.5, 125.3, 125.6, 125.9, 126.6, 127.2 (7 × pyrene-*C*H), 127.9 (pyrene-C_q), 128.2, 128.3 (2 × pyrene-*C*H), 130.2, 130.7, 130.8, 131.6 (4 × pyrene-C_q), 131.8, 137.8 (2 × imidazole-C_q), 158.5, 158.7, 166.0 (3 × *C*═O); HR-MS (pos. ESI) calcd. for $C_{30}H_{26}N_5O_4^+$ [M + H]$^+$: 520.19793, found: 520.19788.

1-Methyl-4-(1-methyl-4-(pyrene-1-carboxamido)-1*H*-pyrrole-2-carboxamido)-1*H*-imidazole-2-carboxylic acid (16). The ester **15** (250 mg, 0.48 mmol) and lithium hydroxide (60.6 mg, 1.44 mmol) were dissolved in THF/water (V_1:V_2 = 4 : 1, 15 ml) and stirred for 6.5 h at room temperature. Afterwards the solution was acidified with concentrated hydrochloric acid to pH = 1 and immediately a solid precipitated. It was filtered off and lyophilised from water (10 ml) yielding **16** (180 mg, 0.37 mmol, 77%) as a slightly yellow solid. Mp > 230 °C; IR (KBr-pellet): ν_{max}/cm^{-1} = 2927 (m), 2851 (w), 2361 (s), 2339 (s), 1637 (s), 1543 (s), 1431 (m), 1343 (m), 1264 (m), 1101 (w), 487 (s), 460 (s); ^{1}H NMR (400 MHz, [D$_6$]DMSO, 25 °C): δ_H = 1.07 (9H, J = 7.20 Hz, C*H*$_3$, HNEt$_3^+$), 2.70–2.87 (m, 6H, C*H*$_2$, HNEt$_3^+$), 3.92 (s, 3H, N–C*H*$_3$, imidazole), 3.94 (s, 3H, N–C*H*$_3$, pyrrole), 7.15 (d, 1H, J = 1.67 Hz, pyrrole-C*H*), 7.36 (s, 1H, imidazole-C*H*), 7.58 (d, 1H, J = 1.61 Hz, pyrrole-C*H*), 8.14 (t, 1H, J = 7.65 Hz, pyrene-C*H*), 8.20–8.32 (m, 4H, pyrene-C*H*), 8.34–8.41 (m, 3H, pyrene-C*H*), 8.49 (d, 1H, J = 9.27 Hz, pyrene-*CH*), 10.56 (s, 1H, N*H*), 10.72 (s, 1H, N*H*). ^{13}C NMR (100 MHz, [D$_6$]DMSO, 25 °C): δ_C = 9.28 (3C, *C*H$_3$, HNEt$_3^+$), 36.3 (N–*C*H$_3$. imidazole), 36.3 (N–*C*H$_3$, pyrrole), 45.3 (3C, *C*H$_2$, HNEt$_3^+$), 105.3

This journal is © The Royal Society of Chemistry 2011

(pyrrole-*C*H), 114.9 (imidazole-*C*H), 119.4 (pyrrole-*C*H), 122.3, 122.5 (2 × pyrrole-C_q), 123.7, 123.8 (2 × pyrene-C_q), 124.4, 124.6, 125.3, 125.6, 125.9, 126.6, 127.2 (7 × pyrene-*C*H), 127.9 (pyrene-C_q), 128.2, 128.3 (2 × pyrene-*C*H), 130.2, 130.7, 130.8, 131.6 (4 × pyrene-C_q), 131.8, 138.0 (2 × imidazole-C_q), 158.5, 158.5, 166.0 (3 × *C*═O); EI-MS *m/z* (%) = 447.1 (23.34) $[M - CO_2]^{\bullet+}$, 351.1 (7.50) $[M - C_5H_6N_3O_2]^{\bullet+}$, 229.1 (100.00) $[M - C_{11}H_{12}N_5O_3]^{\bullet+}$.

***tert*-Butyl 4-(1-methyl-4-(1-methyl-4-(pyrene-1-carboxamido)-1*H*-pyrrole-2-carboxamido)-1*H*-imidazole-2-carboxamido)butylcarbamate (17).** The carboxylic acid **16** (104 mg, 0.21 mmol), PyBOP (110 mg, 0.21 mmol) and NMM (70 µl, 0.64 mmol) were dissolved in DMF (3 ml) and stirred for 30 min at room temperature to generate the active ester. After addition of the amine **9** (60.0 mg, 0.32 mmol), the reaction mixture was stirred for an additional 25 h at room temperature. Afterwards the solution was poured onto water (20 ml) and stirred for 2 h at 0 °C. The precipitated solid was filtered off and lyophilised from water (5 ml). The desired product **17** (88.5 mg, 0.13 mmol, 62%) was obtained as a slightly yellow solid. Mp 146–147 °C; IR (KBr-pellet): ν_{max}/cm^{-1} = 2972 (w), 2932 (w), 2861 (w), 2358 (m), 2332 (m), 1739 (m), 1717 (m), 1655 (s), 1533 (s), 1445 (m), 1365 (m), 1098 (w), 488 (m); ^{1}H NMR (400 MHz, [D$_6$]DMSO, 25 °C): δ_H = 1.33–1.42 (m, 2H, imidazole-CO-NH-CH$_2$-CH$_2$-CH$_2$-CH$_2$), 1.35 (s, 9H, C*H*$_3$, ^{t}Bu), 1.42–1.51 (m, 2H, imidazole-CO-NH-CH$_2$-CH$_2$-CH$_2$-CH$_2$), 2.87–2.95 (m, 2H, imidazole-CO-NH-CH$_2$-CH$_2$-CH$_2$-CH$_2$), 3.18–3.25 (m, 2H, imidazole-CO-NH-CH$_2$-CH$_2$-CH$_2$-CH$_2$), 3.94 (s, 3H, N–C*H*$_3$, imidazole), 3.94 (s, 3H, N–C*H*$_3$, pyrrole), 6.75–6.81 (m, 1H, N*H*), 7.15 (d, 1H, *J* = 1.83 Hz, pyrrole-C*H*), 7.51 (s, 1H, imidazole-C*H*), 7.57 (d, 1H, *J* = 1.78 Hz, pyrrole-C*H*), 7.93 (br. t, 1H, *J* = 5.96 Hz, N*H*), 8.14 (t, 1H, *J* = 7.64 Hz, pyrene-C*H*), 8.20–8.32 (m, 4H, pyrene-C*H*), 8.35–8.42 (m, 3H, pyrene-C*H*), 8.49 (d, 1H, *J* = 9.29 Hz, pyrene-*CH*), 10.34 (s, 1H, N*H*), 10.73 (s, 1H, N*H*); ^{13}C NMR (100 MHz, [D$_6$]DMSO, 25 °C): δ_C = 26.6 (imidazole-CO-NH-CH$_2$-CH$_2$-CH$_2$-CH$_2$), 27.0 (imidazole-CO-NH-CH$_2$-CH$_2$-CH$_2$-CH$_2$), 28.2 (3C, *C*H$_3$, ^{t}Bu), 34.8 (N–*C*H$_3$, imidazole), 36.3 (N–*C*H$_3$, pyrrole), 38.0 (imidazole-CO-NH-CH$_2$-CH$_2$-CH$_2$-CH$_2$), 77.3 (C_q, ^{t}Bu), 105.4 (pyrrole-*C*H), 114.3 (imidazole-*C*H), 119.6 (pyrrole-*C*H), 122.2, 122.4 (2 × pyrrole-C_q), 123.7, 123.8 (2 × pyrene-C_q), 124.4, 124.5, 125.3, 125.7, 125.9, 126.6, 127.2 (7 × pyrene-*C*H), 127.9 (pyrene-C_q), 128.3, 128.4 (2 × pyrene-*C*H), 130.2, 130.7, 131.6, 131.8 (4 × pyrene-C_q), 134.1, 136.0 (2 × imidazole-C_q), 158.6, 158.7, 166.0 (3 × *C*═O); HR-MS (pos. ESI) calcd. for $C_{37}H_{40}N_7O_5^+$ $[M + H]^+$: 662.30854, found: 662.30724.

4-(1-Methyl-4-(1-methyl-4-(pyrene-1-carboxamido)-1*H*-pyrrole-2-carboxamido)-1*H*-imidazole-2-carboxamido)butan-1-aminium 2,2,2-trifluoroacetate (18). The protected compound **17** (119 mg, 0.18 mmol) was dissolved in TFA (4 ml) and stirred at room temperature for 6 h. After removal of remaining TFA under reduced pressure, the residual oil was lyophilised from water (10 ml). The desired product **18** (120 mg, 0.18 mmol, quant.) was obtained as a slightly yellow solid. Mp > 230 °C; IR (KBr-pellet): ν_{max}/cm^{-1} = 2954 (w), 2923 (w), 2865 (w), 1738 (w), 1677 (m), 1657 (m), 1560 (s), 1545 (m), 1437 (m) 1203 (m), 1138 (s), 461 (m), 435 (s); ^{1}H NMR (400 MHz, [D$_6$]DMSO, 25 °C): δ_H = 1.49–1.61 (m, 4H, imidazole-CO-NH-CH$_2$-CH$_2$-CH$_2$-CH$_2$), 2.74–2.87 (m, 2H, imidazole-CO-NH-CH$_2$-CH$_2$-CH$_2$-CH$_2$), 3.20–3.33 (m, 2H, imidazole-CO-NH-CH$_2$-CH$_2$-CH$_2$-CH$_2$), 3.94 (s, 3H, N–C*H*$_3$, imidazole), 3.95 (s, 3H, N–C*H*$_3$, pyrrole), 7.17 (d, 1H, *J* = 1.84 Hz, pyrrole-C*H*), 7.52 (s, 1H, imidazole-C*H*), 7.55 (d, 1H, *J* = 1.76 Hz, pyrrole-C*H*), 7.67 (br. s, 3H, N*H*$_3^+$), 8.04 (br. t, 1H, *J* = 6.14 Hz, N*H*), 8.14 (t, 1H, *J* = 7.65 Hz, pyrene-C*H*), 8.20–8.32 (m, 4H, pyrene-C*H*), 8.34–8.42 (m, 3H, pyrene-C*H*), 8.49 (d, 1H, *J* = 9.28 Hz, pyrene-*CH*), 10.28 (s, 1H, N*H*), 10.73 (s, 1H, N*H*); ^{13}C NMR (100 MHz, [D$_6$]DMSO, 25 °C): δ_C = 24.4 (imidazole-CO-NH-CH$_2$-CH$_2$-CH$_2$-CH$_2$), 26.2 (imidazole-CO-NH-CH$_2$-CH$_2$-CH$_2$-CH$_2$), 34.9 (N-*C*H$_3$, imidazole), 36.3 (N-*C*H$_3$, pyrrole), 37.6 (imidazole-CO-NH-CH$_2$-CH$_2$-CH$_2$-CH$_2$), 38.6 (imidazole-CO-NH-CH$_2$-CH$_2$-CH$_2$-CH$_2$), 105.5 (pyrrole-*C*H), 114.6 (imidazole-*C*H), 119.6 (pyrrole-*C*H), 122.2, 122.4 (2 × pyrrole-C_q), 123.7, 123.8 (2 × pyrene-C_q), 124.4, 124.5, 125.3, 125.7, 125.9, 126.6, 127.2 (7 × pyrene-*C*H), 127.9 (pyrene-C_q), 128.3, 128.4 (2 × pyrene-*C*H), 130.2 (pyrene-C_q), 130.2 (C_q, CF_3COO^-), 130.7, 131.6, 131.8 (3 × pyrene-C_q), 134.0, 136.0 (2 × imidazole-C_q), 158.2 (*C*═O, CF_3COO^-), 158.6, 158.7, 166.0 (3 × *C*═O); HR-MS (pos. ESI) calcd. for $C_{32}H_{32}N_7O_3^+$ $[M]^+$: 562.25611, found: 562.25612.

***N*^{2}-(*N*-(*tert*-Butoxycarbonyl)carbamimidoyl)-*N*^{5}-(4-(1-methyl-4-(1-methyl-4-(pyrene-1-carboxamido)-1*H*-pyrrole-2-carboxamido)-1*H*-imidazole-2-carboxamido) butyl)-1*H*-pyrrole-2,5-dicarboxamide.** The salt (**18**; 120 mg, 0.18 mmol), the carboxylate (**12**; 70.7 mg, 0.18 mmol), PyBOP (92.5 mg, 0.18 mmol) and NMM (59.0 µl, 0.54 mmol) were dissolved in DMF (5 ml) and stirred for 20 h at room temperature. Afterwards the solution was poured onto water (15 ml) and stirred for 2 h at 0 °C. The precipitated solid was filtered off, lyophilised from water (5 ml) and purified by flash chromatography (SiO_2, dichloromethane/ethyl acetate = 1/1, + 5% methanol). The desired product **19** (87.4 mg, 0.10 mmol, 56%) was obtained as a yellow solid. Mp > 230 °C; IR (KBr-pellet): ν_{max}/cm^{-1} = 2974 (w), 2929 (m), 2857 (w), 2359 (m), 2337 (m), 1729 (m), 1630 (s), 1527 (s), 1464 (m), 1442 (m) 1286 (s), 1236 (s), 1143 (s), 846 (s), 757 (s); ^{1}H NMR (400 MHz, [D$_6$]DMSO, 25 °C): δ_H = 1.43 (s, 9H, C*H*$_3$, ^{t}Bu), 1.49–1.60 (m, 4H, imidazole-CO-NH-CH$_2$-CH$_2$-CH$_2$-CH$_2$), 3.20–3.29 (m, 4H, imidazole-CO-NH-CH$_2$-CH$_2$-CH$_2$-CH$_2$), 3.94 (s, 3H, N–C*H*$_3$, imidazole), 3.95 (s, 3H, N–C*H*$_3$, pyrrole), 6.70 (br. s, 1H, pyrrole-C*H*), 6.75 (s, 1H, pyrrole-C*H*), 7.14 (d, 1H, *J* = 1.84 Hz, pyrrole-C*H*), 7.51 (s, 1H, imidazole-C*H*), 7.57 (d, 1H, *J* = 1.75 Hz, pyrrole-C*H*), 7.96 (br. t, 1H, *J* = 6.00 Hz, N*H*), 8.14 (t, 1H, *J* = 7.65 Hz, pyrene-C*H*), 8.20–8.34 (m, 5H, pyrene-C*H* und N*H*), 8.34–8.41 (m, 3H, pyrene-C*H*), 8.48 (d, 1H, *J* = 9.28 Hz, pyrene-*CH*), 9.35 (br. s, 1H, N*H*), 10.33 (s, 1H, N*H*), 10.69 (br. s, 1H, N*H*), 10.72 (s, 1H, N*H*), 10.92 (br. s, 1H, N*H*); ^{13}C NMR (100 MHz, [D$_6$]DMSO, 25 °C): δ_C = 26.7 (imidazole-CO-NH-CH$_2$-CH$_2$-CH$_2$-CH$_2$), 26.8 (imidazole-CO-NH-CH$_2$-CH$_2$-CH$_2$-CH$_2$), 27.7 (3C, *C*H$_3$, ^{t}Bu), 34.8 (N–*C*H$_3$, imidazole), 36.3 (N–*C*H$_3$, pyrrole), 38.0 (imidazole-CO-NH-CH$_2$-CH$_2$-CH$_2$-CH$_2$), 38.4 (imidazole-CO-NH-CH$_2$-CH$_2$-CH$_2$-CH$_2$), 105.4 (pyrrole-*C*H), 111.6 (imidazole-*C*H), 114.3, 114.3, 119.6 (3 × pyrrole-*C*H), 122.2, 122.4 (2 × pyrrole-C_q), 123.7, 123.8 (2 × pyrene-C_q), 124.4, 124.5, 125.3, 125.6, 125.9, 126.6, 127.2 (7 × pyrene-*C*H), 127.9 (pyrene-C_q), 128.2, 128.3 (2 × pyrene-*C*H), 130.2, 130.7, 131.6, 131.8 (4 × pyrene-C_q), 134.1, 136.0 (2 × imidazole-C_q), 158.6, 158.7, 159.5, 165.9 (4 × *C*═O); HR-MS (pos. ESI) calcd. for $C_{44}H_{46}N_{11}O_7^+$ $[M + H]^+$: 840.35762, found: 840.35605.

Amino(5-(4-(1-methyl-4-(1-methyl-4-(pyrene-1-carboxamido)-1*H*-pyrrole-2-car-boxamido)-1*H*-imidazole-2-carboxamido)-butylcarbamoyl)-1*H*-pyrrole-2-carbox-amido)methaniminium 2,2,2-trifluoroacetate (4). The protected hybrid compound **19** (51 mg, 60.7 μmol) was dissolved in TFA (2 ml) and stirred at room temperature for 27 h. After removal of remaining TFA under reduced pressure, the residual oil was lyophilised from water (3 ml). The desired product **4** (51.8 mg, 60.7 μmol, quant) was obtained as a yellow solid: Mp 226–228 °C (degradation); IR (KBr-pellet): ν_{max}/cm^{-1} = 3384 (w), 2958 (w), 2931 (w), 2860 (w), 2371 (m), 2348 (m), 1685 (s), 1653 (m), 1639 (m), 1560 (s), 1439 (m), 1200 (s), 1136 (s), 483 (s); ^{1}H NMR (400 MHz, [D$_6$]DMSO, 25 °C): δ_H = 1.49–1.59 (m, 4H, imidazole-CO-NH-CH$_2$-CH$_2$-CH$_2$-CH$_2$), 3.21–3.35 (m, 4H, imidazole-CO-NH-CH$_2$-CH$_2$-CH$_2$-CH$_2$), 3.94 (s, 3H, N–C*H*$_3$, imidazole), 3.94 (s, 3H, N–C*H*$_3$, pyrrole), 6.84–6.88 (m, 1H, pyrrole-C*H*), 7.00–7.05 (m, 1H, pyrrole-C*H*), 7.17 (d, 1H, *J* = 1.86 Hz, pyrrole-C*H*), 7.52 (s, 1H, imidazole-C*H*), 7.55 (d, 1H, *J* = 1.74 Hz, pyrrole-C*H*), 7.98 (br. t, 1H, *J* = 5.83 Hz, N*H*), 8.11–8.33 (m, 9H, pyrene-C*H*, N*H*$_2$ and N*H*$_2^+$), 8.34–8.45 (m, 4H, pyrene-C*H* and N*H*), 8.48 (d, 1H, *J* = 9.28 Hz, pyrene-*CH*), 10.32 (s, 1H, N*H*), 10.72 (s, 1H, N*H*), 10.98 (s, 1H, N*H*), 12.34 (s, 1H, N*H*); ^{13}C NMR (100 MHz, [D$_6$]DMSO, 25 °C): δ_C = 26.5 (imidazole-CO-NH-CH$_2$-CH$_2$-CH$_2$-CH$_2$), 26.8 (imidazole-CO-NH-CH$_2$-CH$_2$-CH$_2$-CH$_2$), 34.9 (N–*C*H$_3$, imidazole), 36.3 (N–*C*H$_3$, pyrrole), 38.0 (imidazole-CO-NH-CH$_2$-CH$_2$-CH$_2$-CH$_2$), 38.5 (imidazole-CO-NH-CH$_2$-CH$_2$-CH$_2$-CH$_2$), 105.4 (pyrrole-*C*H), 112.2 (imidazole-*C*H), 114.4, 115.4, 119.6 (3 × pyrrole-*C*H), 122.2, 122.4 (2 × pyrrole-*C*$_q$), 123.7, 123.8 (2 × pyrene-*C*$_q$), 124.4, 124.5 (2 × pyrene-*C*H), 125.3 (pyrrole-*C*$_q$), 125.3, 125.7, 125.9, 126.6, 127.2 (5 × pyrene-*C*H), 127.9 (pyrene-*C*$_q$), 128.3, 128.4 (2 × pyrene-*C*H), 130.2, 130.7, 131.7, 131.8 (4 × pyrene-*C*$_q$), 132.8 (pyrrole-*C*$_q$), 134.1, 136.0 (2 × imidazole-*C*$_q$), 155.0 (guanidine-*C*$_q$), 158.6, 158.7, 159.0, 159.5, 166.0 (5 × *C*═O); HR-MS (pos. ESI) calcd. for $C_{39}H_{38}N_{11}O_5^+$ $[M]^+$: 740.30519, found: 740.30519; HPLC, LC-18 reversed phase, isocratic: methanol, + 0.1% TFA: 290 nm: retention time 13.26 min, relative area 97.37% → corrected yield: 50.4 mg, 59.0 μmol, 97%; 220 nm: retention time 13.27 min, relative area 95.21% → corrected yield: 49.3 mg, 57.7 μmol, 95%.

Spectroscopic studies

Notes: Polynucleotides were purchased as noted: poly dA-poly dT, poly dAdT-poly dAdT, poly dGdC-poly dGdC, poly rA-poly rU (Sigma), calf thymus (ct)-DNA (Aldrich). Polynucleotides were dissolved in Na-cacodylate buffer, *I* = 0.05 mol dm^{-3}, pH = 7. Calf thymus (ct)-DNA was additionally sonicated and filtered through a 0.45 μm filter. Polynucleotide concentration was determined spectroscopically as a concentration of phosphates.[18]

The electronic absorption spectra were obtained on a Varian Cary 100 Bio spectrometer, CD spectra were collected on the Jasco J-810 spectrometer and fluorescence spectra were recorded on a Varian Cary Eclipse fluorimeter; all in quartz cuvettes (1 cm). The measurements were performed in aqueous buffer solution (pH = 7 - Na-cacodylate buffer, *I* = 0.05 mol dm^{-3}, pH = 5 - sodium citrate buffer, *I* = 0.03 M). Under the experimental conditions used the absorbance and fluorescence intensities of studied compounds were proportional to their concentration. The sample concentration in fluorescence measurements had an optical absorbance below 0.05 at the excitation wavelength. In fluorimetric titrations, an excitation wavelength of $\lambda_{exc} > 320$ nm was used to avoid inner filter effects caused by absorption of excitation light by added polynucleotide. The binding constant (K_s) and [bound compound]/[polynucleotide phosphate] ratio (*n*) were calculated according to the Scatchard equation by non-linear least-square fitting, giving excellent correlation coefficients (>0.999) for obtained values for K_s and *n*. Thermal melting curves for ds-polynucleotides and their complexes with studied compounds were determined as previously described by following the absorption change at 260 nm as a function of temperature.[19] The absorbance of studied compound was subtracted from every curve, and the absorbance scale was normalized. Obtained T_m values are the midpoints of the transition curves, determined from the maximum of the first derivative or graphically by a tangent method. Given ΔT_m values were calculated subtracting T_m of the free nucleic acid from T_m of the complex. Every ΔT_m value reported here was the average of at least two measurements, the error in ΔT_m is ± 0.5 °C.

Molecular modelling method

Compound **2** was manually intercalated into the space between two base pairs of double stranded DNA (poly dAdT-poly dAdT) and compounds **3** and **4** were placed into the DNA minor groove. For this purpose we constructed a 13 base pair DNA (poly dAdT-poly dAdT with one dC-dG base pair on the each end for better stability) with the program NUCGEN, a part of the Amber program suit.[20] Compounds **2**, **3** and **4** were built using the module 'Builder' within the program InsightII.[21] The ds-DNA-**2** complex was built by inserting the pyrene moiety of **2** into the gap made by removing a base pair in the middle of ds-DNA, the DNA backbone was connected in a common way and the complete complex was minimised to assure common bond lengths within ds-DNA. The AMBER ff99 force field of Duan *et al.*[22] and the general AMBER force field GAFF were used to parameterize the substrate-DNA complexes. Each of the complexes was placed in the centre of the octahedral box filled with TIP3P type water molecules, a water buffer of 7 Å was used, and Na^+ ions were added to neutralize the systems. The solvated complexes were geometry optimized using the steepest descent and conjugate gradient methods, 2500 steps of each, and equilibrated for 0.5 ns. During equilibration the temperature was gently increased from 0 to 300 K and the volume was kept constant. The equilibrated systems were subjected to 12.5 ns (complex with **2**) and 10.5 ns (complexes with **3** and **4**) of the productive molecular dynamics (MD) simulation at constant temperature and pressure (300 K, 1 atm). No restraints were used during the productive MD simulations. The time step during the simulation was 1 fs and the temperature was kept constant using Langevin dynamics with a collision frequency of 1 ps^{-1}.

Geometry optimisation and molecular dynamics (MD) simulations were accomplished using the AMBER 9 program package. The simulation was accomplished using Periodic Boundary Conditions (PBC). The Particle Mesh Ewald (PME) method was used for calculation of the long range electrostatic interactions. In the direct space the pairwise interactions were calculated within the cutoff-distance of 11 Å.

 This journal is © The Royal Society of Chemistry 2011

Proliferation assays

The growth inhibition activity was assessed as described previously,[23] according to the slightly modified procedure of the National Cancer Institute, Developmental Therapeutics Program.[24] The cells were inoculated onto standard 96-well microtiter plates on day 0. Test agents were then added in five consecutive 10-fold dilutions and incubated for a further 72 h. Working dilutions were freshly prepared on the day of testing. The solvent (DMSO) was also tested for eventual inhibitory activity by adjusting its concentration to be the same as in working concentrations (maximal concentration of DMSO was 0.25%). After 72 h of incubation, the cell growth rate was evaluated by performing the MTT assay which detects dehydrogenase activity in viable cells. The absorbency (OD, optical density) was measured on a microplate reader at 570 nm. Each test point was performed in quadruplicate in three individual experiments. The results are expressed as IC_{50}, which is the concentration necessary for 50% of inhibition. The IC_{50} values for each compound are calculated from dose-response curves using linear regression analysis by fitting the test concentrations that give PG values above and below the reference value (*i.e.* 50%). Each result is a mean value from three separate experiments.

Acknowledgements

C.S. thanks the DFG (Deutsche Forschungsgemeinschaft) and the Fonds of the Chemical Industry for ongoing financial support of his work. I.P., S.T. and M.K. thank the Ministry of Science, Education and Sport of Croatia for financial support of this study (Projects 098-0982914-2918, 098-1191344-2860, 098-0982464-2514). We also acknowledge the support from a bilateral funding project between the DAAD and the Ministry of Science, Education and Sport of Croatia.

Notes and references

1 R. B. Silverman, *The Organic Chemistry of Drug Design and Drug Action*, Elsevier Academic Press, New York, 2004.
2 M. Demeunynck, C. Bailly, W. D. Wilson, ed. *DNA and RNA Binders*; Wiley-VCH: Weinheim, 2002.
3 E. Trinquet and G. Mathis, *Mol. BioSyst.*, 2006, **2**, 380.
4 L. Hernandez-Folgado, C. Schmuck, S. Tomić and I. Piantanida, *Bioorg. Med. Chem. Lett.*, 2008, **18**, 2977–2981.
5 L. Hernandez-Folgado, D. Baretić, I. Piantanida, M. Marjanović, M. Kralj, T. Rehm and C. Schmuck, *Chem.–Eur. J.*, 2010, **16**, 3036–3056.
6 P. B. Dervan, *Bioorg. Med. Chem.*, 2001, **9**, 2215–2235.
7 E. E. Baird and P. B. Dervan, *J. Am. Chem. Soc.*, 1996, **118**, 6141–6146.
8 C. Schmuck, V. Bickert, M. Merschky, L. Geiger, D. Rupprecht, J. Dudaczek, P. Wich, T. Rehm and U. Machon, *Eur. J. Org. Chem.*, 2008, 324–329.
9 G. Malojčić, I. Piantanida, M. Marinić, M. Žinić, M. Marjanović, M. Kralj, K. Pavelić and i H.-J. Schneider, *Org. Biomol. Chem.*, 2005, **3**, 4373–4381.
10 C. R. Cantor and P. R. Schimmel, *Biophysical Chemistry*, vol. 3. WH Freeman and Co., San Francisco, 1980, 1109–1181.
11 G. Scatchard, *Ann. N. Y. Acad. Sci.*, 1949, **51**, 660–672; J. D. McGhee and P. H. von Hippel, *J. Mol. Biol.*, 1976, **103**, 679–684.
12 A. Rodger, B. Norden, In *Circular Dichroism and Linear Dichroism*; Oxford University Press: New York, 1997, Chapter 2.
13 N. Berova, K. Nakanishi, R. W. Woody (2000) *Circular dichroism Principles and Applications*, 2nd edn, New York Wiley-VCH.
14 M. Eriksson and B. Nordén, *Methods in Enzymology*, Vol 340, 2001, Pages 68–98, Table I.
15 B. Norden and F. Tjerneld, *Biopolymers*, 1982, **21**, 1713–1734; R. Lyng, A. Rodger and B. Norden, *Biopolymers*, 1991, **31**, 1709–1820; P. E. Schipper, B. Norden and F. Tjerneld, *Chem. Phys. Lett.*, 1980, **70**, 17–21.
16 W. D. Wilson, Y.-H. Wang, C. R. Krishnamoorthy and J. C. Smith, *Biochemistry*, 1985, **24**, 3991–3999.
17 H. S Koo, H. M Wu and D. M Crothers, *Nature*, 1986, **320**, 501–506; D. MacDonald, K. Herbert, X. ZZhang, T. Polgruto and P. Lu, *J. Mol. Biol*, 2001, **5**, 1081–1098.
18 M. Radić Stojković and I. Piantanida, *Tetrahedron*, 2008, **64**, 7807–7814.
19 J.-L. Mergny and L. Lacroix, *Oligonucleotides*, 2003, **13**, 515–537.
20 http://amber.scripps.edu/.
21 INSIGHTII – Accelerys San Diego 2001–2008. (http://accelrys.com/services/training/life-science/insight-migration.html).
22 Y. Duan, C. Wu, S. Chowdhury, M. C. Lee, G. Xiong, W. Zhang, R. Yang, P. Cipelak, R. Luo and T. Lee, A point-charge force field for molecular mechanics simulations of proteins, *J. Comput. Chem.*, 2003, **24**, 1999–2012.
23 M. Marjanović, M. Kralj, F. Supek, L. Frkanec, I. Piantanida, T. Šmuc and L. Tušek-Bo,žić, *J. Med. Chem.*, 2007, **50**, 1007–1018.
24 M. R. Boyd and D. P. Kenneth, *Drug Dev. Res.*, 1995, **34**, 91–109.